# A COMPARISON OF THEORY AND EXPERIMENT FOR THE AEROELASTIC STABILITY OF A BEARINGLESS MODEL ROTOR IN HOVER



Seth Dawson
U.S. Army Aeroflightdynamics Directorate
Ames Research Center



## Abstract

Three cases were selected for correlation from an experiment that examined the aeroelastic stability of a small-scale bearingless model rotor in hover. The 1.8-m diameter model rotor included flap, lead-lag, and torsional degrees of freedom, but no body degrees of freedom. The first case looked at a configuration with a single pitch link on the leading edge, the second case examined a configuration with a single pitch link on the trailing edge, and the third case examined a configuration with pitch links on the leading and trailing edges to simulate a pitch link with shear restraint. Analyses from Bell Helicopter Textron, Boeing Vertol, Hughes Helicopters, Sikorsky Aircraft, and the U.S. Army Aeromechanics Laboratory were compared with the data, and the correlation ranged from poor to fair.

## Introduction

As a part of the Methodology Assessment, three cases were selected from the experiments reported in Ref. 1 for comparison with theoretical models. Each of the selected cases used the same blades and flexbeams; the only differences between the cases was in the pitch link configuration. Case 1 used a single pitch link on the leading edge, Case 2 used a pitch link on the trailing edge, and Case 3 had pitch links on both leading and trailing edges to simulate a pitch link with shear restraint. As the control configuration was the only variable between the three cases, it is possible to assess the capabilities of the analytical models to represent the effects of control configuration on stability, effects that are particularly important for bearingless rotor designs.

The theoretical models compared with some or all of the data included the Bell Helicopter Textron DRAV21 analysis; Boeing Vertol C-90 analysis; the Hughes Helicopters DART model; the G400 analysis and two versions of E927 used by Sikorsky Aircraft; and the U.S. Army Aeromechanics Laboratory FLAIR analysis.

The paper will briefly describe the experiment from which these data were obtained and then present the correlation. Conclusions will be made as to the quality of the agreement between theory and experiment. Appendices are provided that document the experimental model properties, tabulate the experimental data points, and show all of the correlations.

## Description of Experiment

A two-bladed bearingless model rotor with a diameter of 1.8 m (5.88 ft) was tested in hover to obtain the experimental data. The experiment has been previously reported in Ref. 1. The model, which is shown in Fig. 1, was designed to match as closely as possible characteristics of the U.S. Army Aeromechanics Laboratory FLAIR program. The blades are attached to the hub using a Kevlar 49 flexbeam of rectangular cross-section that extends from an 8.7% to 19.9% radius. The exploded view of Fig. 2 shows the configuration with pitch links on the leading and trailing edge (Case 3); however, either pitch link may be removed to give a single pitch-link configuration. The pitch links are designed to minimize nonlinear structural damping by using flexural elements on either end instead of rod end bearings. Flexbeam precone and pitch angle

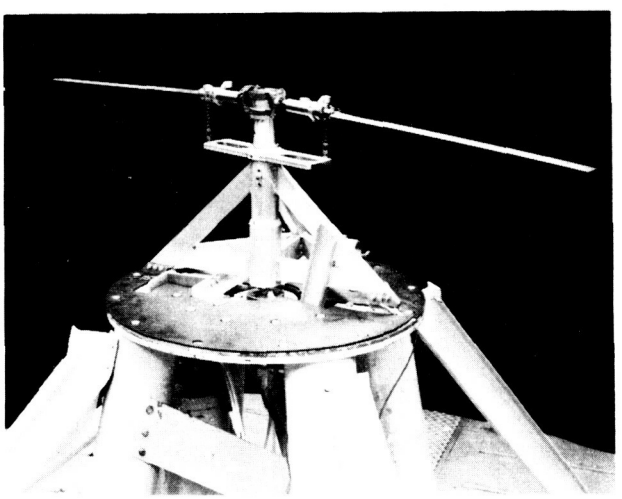

Fig. 1 Two-bladed bearingless model rotor.

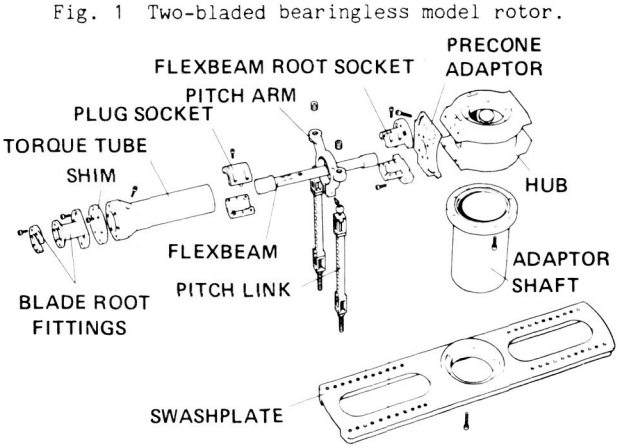


Fig. 2 Exploded view of bearingless model rotor flexbeam and hub.

with respect to the hub may be independently varied with the precone adaptor and flexbeam root socket. Blade prepitch and precone changes with respect to the flexbeam may be made independently with the blade root fittings and a shim. Pitch angle changes are made by raising or lowering the pitch links with respect to the dummy swashplate. This transmits a moment along the torque tube to the outboard end of the flexbeam, twisting the flexbeam, and introduces some flap-lag elastic coupling along with the pitch angle change. The model flexbeams on both blades are instrumented with strain-gage bridges to measure flap, lead-lag, and torsional strain. Rotor properties are given in Table 1.

Table 1 Rotor Properties

| Property | Value |
|---|---|
| Radius, R, in. | 35.51 |
| Blade chord, c, in. | 1.65 |
| Solidity, $\sigma$ | 0.02957 |
| Flexbeam length, in. | 4.0 |
| Flexbeam width, in. | 0.32 |
| Flexbeam thickness, in. | 0.142 |
| Flexbeam tip distance from center, in. | 7.014 |

The rotor test stand consists of a frame that contains the driveshaft, drive sheave, and slip ring, and a lower support structure that houses the drive motor and powers the rotor through a V-belt. The upper frame is connected to the lower support structure with two flexures. A 50-lb electromagnetic shaker is used to excite the upper frame and hub at the blade lead-lag natural frequency. Two pneumatic clamps lock the upper frame following excitation of the lead-lag motion of the blades.

For each test condition the blade pitch angle was set manually by raising or lowering the pitch links. The resulting pitch angle was measured with the blade supported so that the flap bending moment on the flexbeam was zero. The rotor was then brought up to the test condition rotor speed. Transient blade lead-lag motion was induced by unlocking the pneumatic clamps to free tne upper stand, oscillating the rotor hub at the fixed-system, lead-lag natural frequency ($\omega_\zeta + \Omega$) with the shaker, and once sufficient lead-lag motion was obtained, the excitation was stopped and the upper stand clamped. Frequency and damping were determined from the transient decay of the rotor differential lead-lag mode using the moving-block analysis. The blade data were recorded digitally and on analog tape. A complete discussion of the model properties is provided in Appendix A. The measured modal damping used for the correlation is tabulated in Appendix B.

## Correlation

Three cases were selected from the experiment for correlation. The only difference between the cases was the location of the pitch links as shown in Fig. 3. For Case 1, a single pitch link was located on the leading edge at 10% of the flexbeam span. For Case 2, a single pitch link was located at the trailing edge and the same radial location. For Case 3, pitch links were used on the leading and trailing edges of the blade to simulate a single pitch link and vertical shear restraint. For all three configurations, the blade and flexbeam precone and pretwist angles were set to zero.

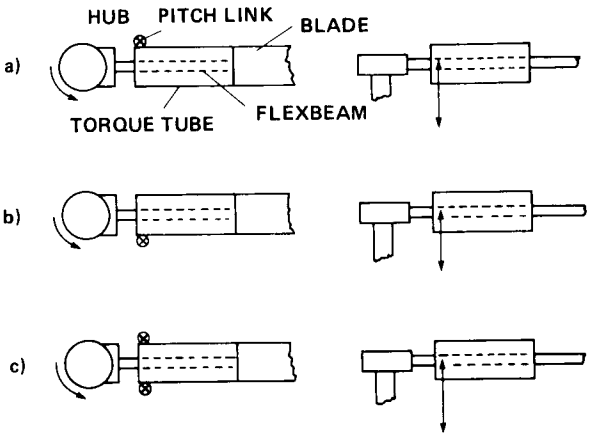


Fig. 3 Bearingless model rotor control configuration. a) Case 1--single pitch link on the leading edge. b) Case 2--single pitch line on the trailing edge. c) Case 3--pitch links on leading and trailing edges.

Two of the companies involved in the correlation effort uncovered problems with the experimental model properties documentation in setting up their analytical models. A comparison of calculated and measured nonrotating frequencies for a check case where no pitch links were mounted to the blade showed a significant underprediction of the flap and lead-lag frequencies (Table 2). It can be seen that Bell Helicopter Textron adjusted the flexbeam EI values to provide a better match of the nonrotating frequencies. However, Sikorsky changed their method of representing the flexbeam end conditions. Boeing Vertol made no change to the flexbeam properties. Hughes Helicopters did not provide nonrotating frequency calculations, and it is not known if they made any adjustments. The U.S. Army Aeromechanics Laboratory took an alternate approach in setting up the FLAIR analysis by defining the flexbeam properties for each case on the basis of a match with nonrotating frequency measurements. A comparison of nonrotating frequency measurements and calculations used for the correlation for the three cases is shown in Table 3.

Table 2 Nonrotating Modal Frequencies for a Configuration without Pitch Links

| | $\omega_{\beta 1}$, Hz | $\omega_{\beta 2}$, Hz | $\omega_{\zeta 1}$, Hz | $\omega_{\theta 1}$, Hz |
|---|---|---|---|---|
| Measurement | 4.69 | 24.81 | 10.94 | 19.73 |
| Bell Helicopter Textron[a] | 4.68 | 25.86 | 11.01 | 21.18 |
| Sikorsky Aircraft, unadjusted[b] | 4.09 | 22.57 | 8.86 | 19.79 |
| Sikorsky Aircraft, adjusted[c] | 4.78 | 25.03 | 10.89 | 19.79 |

[a]Flap stiffness increased 38% and chord stiffness 87% to match nonrotating frequencies.
[b]Using original tabulated stiffnesses.
[c]Adjusting tabulated stiffnesses to correct for flexbeam end effects.

Table 3 Comparison of Measured and Predicted Nonrotating Frequencies

| Case | | $\omega_{\beta 1}$, Hz | $\omega_{\beta 2}$, Hz | $\omega_{\zeta 1}$, Hz | $\omega_{\theta 1}$, Hz |
|---|---|---|---|---|---|
| 1 | Measurement | 4.84 | -- | 10.97 | 39.69 |
| | Bell Helicopter Textron | 4.82 | 25.84 | 11.01 | 45.68 |
| | Boeing Vertol | 4.38 | -- | 8.66 | -- |
| | Sikorsky Aircraft | 4.93 | -- | 10.82 | 47.4 |
| | FLAIR | 4.89 | -- | 11.03 | 38.76 |
| 2 | Measurement | 4.88 | 24.81 | 10.95 | 40.56 |
| | Bell Helicopter Textron | 4.83 | 25.84 | 11.01 | 45.73 |
| | Boeing Vertol | 4.79 | -- | 8.99 | 56.34 |
| | Sikorsky Aircraft | 4.93 | -- | 10.92 | 47.4 |
| | FLAIR | 4.86 | -- | 11.10 | 38.57 |
| 3[a] | Measurement | 6.05 | 24.81 | 10.80 | 173.0 |
| | Boeing Vertol | 4.22 | -- | 8.25 | -- |
| | Sikorsky Aircraft | 6.76 | 26.6 | 10.75 | 193.8 |
| | FLAIR | 6.02 | -- | 11.11 | 179.0 |

[a]Bell Helicopter Textron did not predict Case 3.

Case 1

The Case 1 configuration at 1100 rpm is representative of a soft inplane rotor with a dimensionless lead-lag frequency of 0.74. The single leading edge pitch link is located radially near the root end of the flexbeam. This results in positive pitch-flap coupling (negative $\delta_3$) and therefore the first flapping frequency is predicted to be less than 1/rev. The torsional frequency is calculated to be 2.6/rev.

Six theoretical predictions are compared with the experimental data in Fig. 4. The individual codes are keyed to the caption and the data are shown as a stippled area. Theory and data show the same behavior in general--a minimum in damping at the low pitch angles with the damping increasing with an increase in the absolute value of the pitch angle. The differences between the theoretical predictions and the data are largely seen in the change of damping with blade pitch angle and the location of the damping minimum. In this latter respect, all of the codes except Sikorsky's E927-3 predict the minimum to occur between -2° and 0° pitch, while the data show a mirror image behavior with the minimum at about +2°.

The DRAV21 predictions (BH) show a damping increase that is similar to the data, but the damping minimum occurs at about -2° instead of at +2° and the predicted minimum damping is higher than

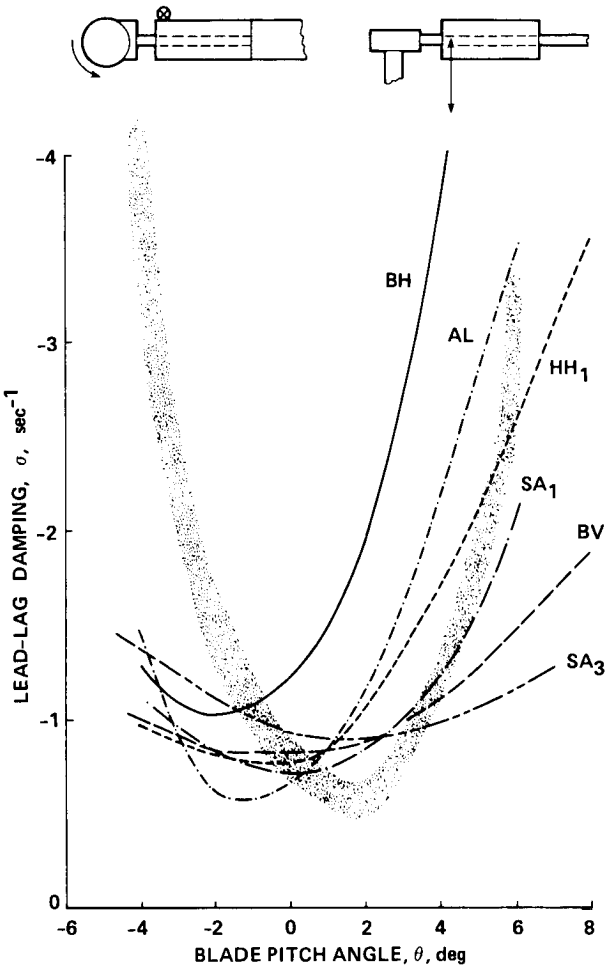


Fig. 4 Composite comparison of theory and experiment for Case 1 for lead-lag mode damping; 1100 rpm. Data are shown as stippled area; analyses used are DRAV21 (BH), C90 (BV), DART ($HH_1$), G400 ($SA_1$), E927-3 ($SA_3$), and FLAIR (AL).

the measurements. Overall the correlation is judged poor. The damping was also predicted using a dynamic inflow model; the results are included in Appendix C. There is perhaps a slight improvement in the agreement, but this is not considered significant.

The C-90 predictions (BV) show substantially less of an increase in damping than the measurements as pitch angle increases. The damping minimum is quite broad and occurs at about 0° rather than +2°. In general the correlation is considered to be poor.

The DART predictions ($HH_1$) show a reasonable agreement in the damping increase for positive pitch angles, but not at negative pitch angles. The damping minimum appears to occur at about 0° rather than +2° and the correlation is judged poor. The pitch angle shown for the DART calculations is the equilibrium or trim pitch angle that results after all steady loads have been applied. This is not directly comparable to the experimental pitch angle measurements which were made statically with the blade supported for zero flap deflection.

Sikorsky predicted the Case 1 lead-lag damping with two analyses: G400 ($SA_1$) and E927-3 ($SA_3$). In both cases NASTRAN was used to calculate the mode shapes and frequencies. The G400 code shows less of a damping increase with pitch angle than the data and predicts the minimum to occur at about 0° rather than +2°. The E927-3 predictions show relatively little variation with pitch angle; however, the damping minimum does appear to occur at about +2°. Although the G400 predictions are considered slightly better than the E927-3 calculations, the correlation for both codes is considered poor.

The Aeromechanics Laboratory FLAIR analysis (AL) shows reasonable agreement in the increase of damping with pitch angle, but as with the majority of the other codes, it shows a shift in the minimum damping to -1° or -2° rather than the measured +2°. However, unlike the other codes, FLAIR shows a fairly rapid increase in the damping at negative pitch angles and for this reason its correlation is considered poor-to-fair.

The disagreement between most of the predictions and the data in the location of the damping minimum for Case 1 is perplexing. The large variation in damping that is seen in this case allows this minimum or damping bucket to be well-defined both experimentally and theoretically. For a purely symmetric rotor it might be expected that the minimum should occur at 0°, but there are a number of asymmetries for Case 1 including blade weight, pitch-flap coupling, and the cambered 23012 airfoil that was used. For the 23012 airfoil, the zero inflow condition occurs at -1.5° although Hughes Helicopters has suggested that the damping should be symmetric about zero inflow. However, the minimum parasite drag angle occurs at a positive 1° to 2° for this airfoil and it is not clear what effect this would have on the location of the damping minimum.

Case 2

The damping as a function of blade pitch angle for Case 2 is compared with the various theoretical predictions in Fig. 5 for a rotor speed of 900 rpm. This corresponds to a measured lead-lag frequency of 0.87/rev. The single pitch link is located on the trailing edge, which results in negative pitch-flap coupling; therefore, the predicted first flap frequency is well above 1/rev. The torsional frequency is calculated to be 3.2/rev (using FLAIR). The rate of change of damping with pitch angle is much less than was seen for Case 1. Lead-lag damping data were not obtained for blade pitch angles of 0° and 2° because of a blade flutter encountered at a rotor speed of approximately 860 rpm.

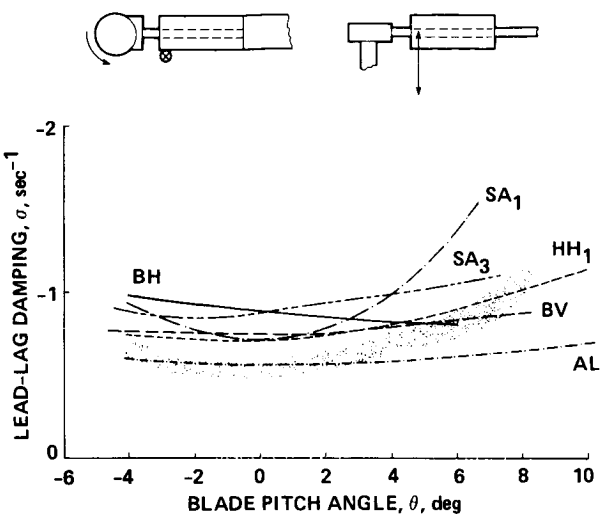


Fig. 5 Composite comparison of theory and experiment for Case 2 for lead-lag mode damping; 900 rpm. Data are shown as stippled area; analyses used are: DRAV21 (BH), C90 (BV), DART ($HH_1$), G400 ($SA_1$), E927-3 ($SA_3$), and FLAIR (AL).

The correlation in this case is improved over Case 1 in general. The DRAV21 analysis (BH) shows a similar damping level to the data but a different slope, and is considered poor-to-fair. The Boeing Vertol C-90 analysis (BV) shows better agreement and is judged fair. The DART analysis ($HH_1$) shows approximately the correct level and a similar slope and is considered fair-to-good. The DART predictions were made at 1100 rpm rather than 900 rpm and it is not known whether calculations made at the correct rotor speed would show improved agreement. The two Sikorsky analyses show a mixed effect with G400 ($SA_1$) showing too much effect of pitch angle and E927-3 ($SA_3$) showing too little variation. Both are rated poor-to-fair. The FLAIR analysis (AL) shows the best agreement at negative and low pitch angles, but does not show the damping increase at the higher pitch angles so is considered fair.

As the basis of comparison for this case was the prediction of lead-lag damping, the damping of other rotor modes was not required. However, it is interesting to note that the DART analysis showed an unstable first torsion mode at pitch angles of -4°, 0°, and +4° which is suggestive of the flutter seen on the model rotor at pitch angles of 0° and +2°. It is not known if the flutter would have been predicted if the correct rotor speed had been used for the DART calculations. In retrospect, the prediction of the experimental flutter should have been included in comparing theory and experiment for Case 2. If this had been the case, an accurate prediction of the flutter condition would result in an improved judgment of the DART analysis.

Case 3

The lead-lag damping as a function of blade angle for Case 3 is shown in Fig. 6. For this 1100-rpm condition, the measured lead-lag frequency is 0.75/rev. The location of the pitch links on the leading and trailing edges stiffens the torsional degree of freedom as compared to Cases 1 and 2 and also avoids pitch-flap coupling. This is reflected in calculated values of the first flap and torsion frequencies of 1.08/rev and 5.8/rev, respectively (using FLAIR). The damping behavior is similar to Case 2, but shows a larger variation in damping as pitch angle is changed. Bell did not provide calculations for this case as the Myklestad program, which provides blade modes for the DRAV21 analysis, is not able to properly model the double-pitch-link case.

The C-90 (BV) and DART ($HH_1$) analyses show very similar behavior for this case. The damping is fairly well predicted for pitch angles near zero, but neither method shows the measured damping increase for pitch angles above 4° and both are considered to be fair. The FLAIR (AL) analysis behaves very much like the C-90 and DART predictions, but is offset to a lower damping and is only considered to be poor-to-fair.

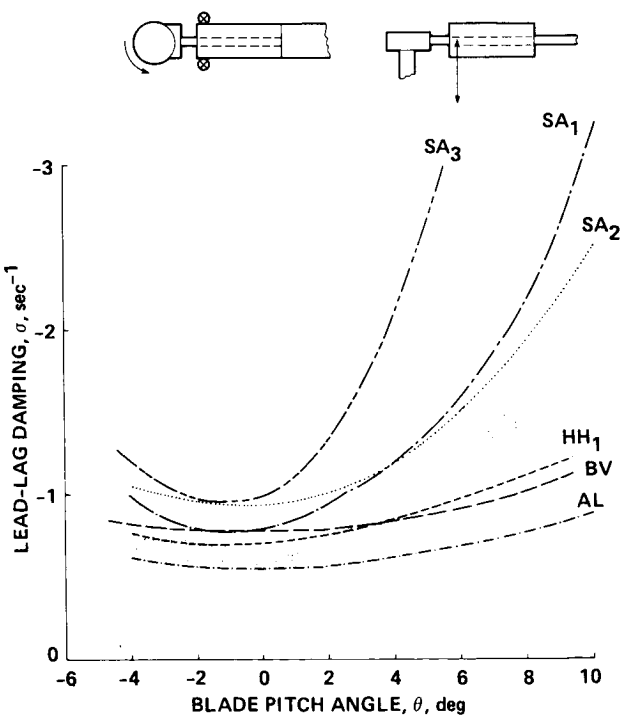


Fig. 6 Composite comparison of theory and experiment for Case 3 for lead-lag mode damping; 1100 rpm. Data are shown by stippled area; analyses used are C90 (BV), DART ($HH_1$), G400 ($SA_1$), E927-2 ($SA_2$), E927-3 ($SA_3$), and FLAIR (AL).

Sikorsky predicted the damping in this case with their G400 analysis and two versions of the E927 code. The G400 ($SA_1$) and E927-2 ($SA_2$) predictions show a behavior that is very similar to the data, but are slightly offset. The agreement in this case is judged to be fair. The E927-3 ($SA_3$) predictions show an excessive sensitivity to pitch angle and are considered to be poor.

## Conclusions

The predictions of six analysis programs were compared with the data for three experimental data sets obtained from an experiment designed to measure the lead-lag damping of an isolated bearingless rotor in hover. Overall, the correlation varied from poor (E927-3) to fair (DART), and in this sense the use of experimental data sets did not act as a strong discriminant between the analytical methods. The fact that none of the prediction methods was able to achieve fair-to-good correlation leaves unresolved the problem of whether the major modeling difficulties lie with the theoretical or experimental efforts.

## References

[1]Dawson, Seth, "An Experimental Investigation of a Bearingless Model Rotor in Hover," Journal of the American Helicopter Society, Vol. 28, No. 4, Oct. 1983, pp. 29-34.

[2]Bousman, William G., "A Comparison of Theory and Experiment for Coupled Rotor-Body Stability of a Hingeless Rotor Model in Hover," NASA CP-10007, May 1988.

[3]Silcox, H. F., "Analytical and Model Investigations of Hingeless Rotor Air Stability, Vol. 1, Section A: Structures Analysis--Rigid Blades," Report D210-10475-1A, Boeing Company, 1972.

## Appendix A--Model Properties

The three cases examined in this paper are from an experiment originally reported in Ref. 1. A limited discussion of model properties was provided in that reference. The present appendix provides a substantially more detailed discussion of the model properties.

### Geometric Properties

The major rotor descriptive properties are given in Table 1. The dimensional data have been obtained from design drawings. The same blade is used as in the experiment discussed in Ref. 2 and the appropriate analytic representation of the aerodynamic section properties for this NACA 23012 airfoil is:

$$C_\ell = 0.15 + 5.73\alpha$$

$$C_d = 0.0079 + 1.7\alpha^2$$

$$C_m = -0.012$$

where the angle of attack, $\alpha$, is in radians.

### Mass and Stiffness Properties

The design drawings of the hub, flexbeam, root hardware, and blade were used to calculate mass, stiffness, and pitching inertia outboard of blade station (B.S.) 1.400 in. This blade station corresponds to the outer edge of the cylindrical section of the hub shown in Fig. 2. The calculated properties of the flexbeam and blade are given in Table 4, and the calculated properties of the torque tube and pitch hardware are shown in Table 5. Torque tube properties are calculated inboard of B.S. 7.014 in., which corresponds to the flexbeam tip. The pitch arm is included, but not the pitch links or their ball sockets. Blade properties outboard of B.S. 8.931 in. were obtained from Ref. 3. The flexbeam and root hardware are centered on the blade quarter chord and therefore inboard of B.S. 7.994 in the center of mass and elastic axis are coincident at 0.25c. The blade outboard of B.S. 7.944 in. was designed to have the center of mass and elastic axis coincident with 0.25c as well. No measurements have been made of the blade elastic axis, but measurements of blade center of mass outboard of B.S. 7.944 in. have ranged from 0.256c to 0.266c with an average value of 0.262c.

Measurements were made of the overall mass properties of the blade and root hardware combination as shown in Table 6. The root hardware included the pitch arm but not the pitch links and a flexbeam was used that had been cut at the centerline (B.S. 5.014 in.). The mass was measured with a conventional laboratory scale and the spanwise c.g. was determined by balancing the blade on a knife edge. The moment of inertia was determined by suspending the blade from its tip and measuring its pendular frequency. These measurements were made in both the flap and chord directions; the variation was ±5.0%. The average value of the moment of inertia is shown in Table 6. Pendular measurements were also used to determine the blade/root hardware pitch inertia by suspending the blade from a point slightly behind its trailing edge. Calculations of the integrated rotor mass properties based on Tables 4 and 5 are compared to the measurements in Table 6. The agreement between calculation and measurement is excellent for the mass, but the calculated location of the blade spanwise c.g. is outboard of the measured location by a quarter of an inch (0.8% of blade radius). The calculated moment of inertia is 2.3% above the measured value, but as the measurements showed a ±5% variation, this difference is not considered

Table 4 Calculated Mass and Stiffness Properties of Flexbeam and Blade[a]

| Blade Station, in. | Weight, $lb_m$/in. | $EI_f$, $10^6$ lb-in.$^2$ | $EI_c$, $10^6$ lb-in.$^2$ | GJ, $10^6$ lb-in.$^2$ | $I_\theta$, $lb_m$-in.$^2$/in. |
|---|---|---|---|---|---|
| 1.400 | 1.70 | 44.9 | 27.3 | 20.7 | 0.704 |
| 1.653 | 0.813 | 37.2 | 25.7 | 17.5 | 0.534 |
| 1.826 | 0.738 | 44.7 | 25.2 | 10.7 | 0.831 |
| 2.159 | 0.862 | 25.4 | 20.6 | 30.2 | 0.449 |
| 2.159 | 0.500 | 72.1 | 72.1 | 10.9 | 0.141 |
| 2.359 | 0.500 | 72.1 | 72.1 | 10.9 | 0.141 |
| 2.359 | 0.180 | 0.863 | 0.863 | 3.76 | 0.0169 |
| 3.014 | 0.180 | 0.863 | 0.863 | 3.76 | 0.0169 |
| 3.014 | 0.147 | 0.00084 | 0.00427 | 0.000066 | 0.0178 |
| 3.159 | 0.147 | 0.00084 | 0.00427 | 0.000066 | 0.0178 |
| 3.159 | 0.00227 | 0.00084 | 0.00427 | 0.000066 | 0.000278 |
| 7.014 | 0.00227 | 0.00084 | 0.00427 | 0.000066 | 0.000278 |
| 7.014 | 0.268 | 3.02 | 3.02 | 2.31 | 0.120 |
| 7.309 | 0.350 | 5.24 | 5.24 | 4.04 | 0.209 |
| 7.644 | 0.350 | 5.24 | 5.24 | 4.04 | 0.209 |
| 7.644 | 0.413 | 8.87 | 8.87 | 6.29 | 0.324 |
| 7.944 | 0.413 | 8.87 | 8.87 | 6.29 | 0.324 |
| 7.944 | 0.222 | 1.77 | 3.66 | 2.18 | 0.0550 |
| 8.005 | 0.220 | 1.77 | 3.66 | 2.18 | 0.0550 |
| 8.005 | 0.220 | 1.77 | 3.66 | 2.18 | 0.0550 |
| 8.134 | 0.231 | 1.77 | 3.66 | 2.18 | 0.0550 |
| 8.134 | 0.0529 | 0.124 | 0.124 | 0.0959 | 0.00247 |
| 8.599 | 0.0510 | 0.124 | 0.124 | 0.0959 | 0.00243 |
| 8.781 | 0.191 | 0.124 | 0.124 | 0.0959 | 0.0394 |
| 8.931 | 0.191 | 0.124 | 0.124 | 0.0959 | 0.0394 |
| 8.931 | 0.0243 | 0.0459 | 0.0459 | 0.0238 | 0.000728 |
| 8.990 | 0.0296 | 0.0538 | 0.0538 | 0.0288 | 0.000867 |
| 8.990 | 0.119 | 0.0538 | 0.0538 | 0.0288 | 0.0147 |
| 9.050 | 0.118 | 0.0991 | 0.0991 | 0.0616 | 0.0155 |
| 9.050 | 0.155 | 0.0991 | 0.0991 | 0.0616 | 0.0195 |
| 9.180 | 0.160 | 0.101 | 0.101 | 0.0596 | 0.0297 |
| 9.180 | 0.0447 | 0.101 | 0.101 | 0.0596 | 0.00172 |
| 9.285 | 0.0470 | 0.102 | 0.102 | 0.0568 | 0.00167 |
| 9.285 | 0.0332 | 0.0526 | 0.0526 | 0.0187 | 0.000684 |
| 9.445 | 0.00763 | 0.00228 | 0.0617 | 0.0012 | 0.000711 |
| 11.445 | 0.00758 | 0.00228 | 0.0617 | 0.0012 | 0.000869 |
| 35.445 | 0.00748 | 0.00228 | 0.0617 | 0.0012 | 0.000869 |

[a]Does not include torque tube, pitch arm, or pitch links.

Materials:

steel: $\rho = 0.283\ lb_m/in.^3$, $E = 29\times10^6$ lb/in.$^2$, $G = 11\times10^6$ lb/in.$^2$

titanium: $\rho = 0.160\ lb_m/in.^3$, $E = 16\times10^6$ lb/in.$^2$, $G = 6.2\times10^6$ lb/in.$^2$

Kevlar: $\rho = 0.050\ lb_m/in.^3$, $E = 11\times10^6$ lb/in.$^2$, $G = 0.3\times10^6$ lb/in.$^2$

Table 5 Calculated Mass and Stiffness Properties of Torque Tube[a]

| Blade Station, in. | Weight, $lb_m$/in. | $EI_f$, $10^6$ lb-in.$^2$ | $EI_c$, $10^6$ lb-in.$^2$ | GJ, $10^6$ lb-in.$^2$ | $I_\theta$, $lb_m$-in.$^2$/in. |
|---|---|---|---|---|---|
| 3.200 | 0.281 | 12.1 | 26.7 | 3.98 | 0.377 |
| 3.600 | 0.281 | 12.1 | 26.7 | 3.98 | 0.377 |
| 3.600 | 0.0578 | 1.75 | 1.75 | 0.746 | 0.0193 |
| 6.872 | 0.0578 | 1.75 | 1.75 | 0.746 | 0.0193 |
| 6.872 | 0.239 | 2.30 | 2.30 | 0.177 | 0.0456 |
| 7.014 | 0.239 | 2.30 | 2.30 | 0.177 | 0.0456 |

[a]Materials:

steel: $\rho = 0.283\ lb_m/in.^3$, $E = 39\times10^6$ lb/in.$^2$, $G = 11\times10^6$ lb/in.$^2$

titanium: $\rho = 0.160\ lb_m/in.^3$, $E = 16\times10^6$ lb/in.$^2$, $G = 6.2\times10^6$ lb/in.$^2$

aluminum: $\rho = 0.101\ lb_m/in.^2$, $E = 10.5\times10^6$ lb/in.$^2$, $G = 4\times10^6$ lb/in.$^2$

Table 6 Hub and Blade Mass Properties

| Quantity | Measured[a] | | Calculated | Error[b] |
|---|---|---|---|---|
| Mass, $lb_m$ | 1.024 | | 1.025 | +0.1% |
| Centroid of mass, in.[c] | 4.37 | 4.64 | +6.2% | |
| Moment of inertia, $lb_m$-in.$^2$ [c] | 74.03 | | 75.70 | +2.3% |
| Pitch inertia, $lb_m$-in.$^2$ | 0.393 | | 0.486 | +23.7% |

[a]Blade and root hardware including pitch arm and flexbeam outboard of B.S. 5.014 in.

[b] $\frac{\text{Calculated - Measured}}{\text{Measured}} \times 100\%$

[c]With respect to flexbeam center, B.S. 5.014 in.

significant. The calculated pitch inertia is 24% above the measurement which is a significant difference. The cause of this difference is not known.

Modal Frequency and Damping

Measurements were made of the rotor first-flap, lead-lag, and torsion-mode frequencies for each case. The measurements were made with the blades mounted on the rotor hub and average values are shown in Table 7 along with some limited measurements of damping. There is no significant effect of pitch link location between the leading edge (Case 1) and the trailing edge (Case 2). However, the addition of the second pitch link increases the first flap frequency by 25% and the torsion frequency is increased by a factor of four.

Additional nonrotating frequency measurements were made for the Case 2 configuration with the blade and root hardware cantilevered from the hub and with two pitch link configurations: a single pitch link on the trailing edge and both pitch links removed. Modal frequencies for these cases are shown in Table 8. For the case without a pitch link, it is possible to calculate approximate first-mode frequencies from beam theory:

$$\omega = \left(\frac{EI}{\ell I_\beta}\right)^{1/2} \quad \text{for flap and chord}$$

and

$$\omega = \left(\frac{GJ}{\ell I_p}\right)^{1/2} \quad \text{for torsion}$$

where the EI and GJ values from Table 4 for the flexbeam span are used to determine stiffness, $I_\beta$ is the blade inertia about the flexbeam center, and $I_p$ is the blade pitch inertia as calculated from Table 4. The calculated flap and chord frequencies in Table 8 are 11.1% and 7.3% higher than the measured values, respectively. This difference is a result of blade flexibility which is not accounted for in the frequency expressions used here and is larger in flap (blade to flexbeam ratio of EI is 2.7) than chord (ratio is 14.4) as expected. The underprediction of the torsional frequency is believed to be caused by inaccuracies in the blade pitch inertia estimate. If the measured value of pitch inertia from Table 6 is used instead of the calculated value, then the predicted frequency will be 20.25 Hz or 2.8% above the measurement.

The tabulated model properties that were originally supplied to the companies in the format of Tables 4 and 5 were based on measured elastic moduli for Kevlar rather than the standard handbook values that are shown in the tables here. The measurements of the elastic moduli were made in consideration of the sensitivity of these parameters to configuration and lay-up for composite materials. However, as discussed in the text in regard to Table 2, some of the analyses underpredicted the nonrotating frequencies, based on these original properties. Similar underpredictions were obtained using the cantilever beam formula for frequency. This difficulty led to a reexamination of the elastic moduli measurements and a rejection of them because of deflection measurement inaccuracies. The standard E and G values now used in Tables 4 and 5 are believed to provide the best estimate of the elastic moduli.

Control System Stiffness

The effective control-system stiffness was estimated from two separate measurements. The first measurement was obtained by cantilevering the torque tube at its outer end and then loading one pitch arm. The resulting value of 3840 lb/in. includes both the torsional flexibility of the torque tube and its flapwise flexibility. The second measurement was obtained by loading a single pitch link/swashplate combination vertically and then measuring its deflection. This measured value was 2690 lb/in. and is caused by both the torsional and flapwise flexibility of the swashplate. The control system stiffness is assumed to be a series-spring summation of these two measurements and, hence, is 1580 lb/in.

## Appendix B--Experimental Data

Tables 9, 10, and 11 show blade pitch angle in degrees and lead-lag damping in $sec^{-1}$ for Cases 1 to 3. These data were obtained in the experiment reported in Ref. 1. The lead-lag mode was excited and the modal frequency and damping were obtained from the transient decay using the moving-block analysis.

## Appendix C--Correlation

All theoretical predictions and experimental data for the three cases are shown in this appendix as Figs. 7 to 12. Some figures from the main text are repeated here for completeness. The data and correlation with theory are presented in two formats. The first format compares the theoretical predictions and experimental data individually for each mathematical model used. In this format the actual calculated points are shown as solid symbols and the fairing between points was calculated by the experiment analysts. The data are shown as open symbols. The second format compares all the theoretical predictions and experimental data on a single composite plot. The theory is shown as the faired curve from the first format and the experimental data are shown as a stippled area.

All plots show the lead-lag damping ($sec^{-1}$) as a function of blade pitch angle (degrees). The sketch above each figure shows the geometry of the rotor for that particular case. A code is used to identify the theoretical predictions for both the individual and composite comparisons and is explained in Table 12.

Table 7 Flexbeam/Blade Modal Frequency and Damping

| Case | Flap | | Lead-lag | | Torsion | |
|---|---|---|---|---|---|---|
| | ω, Hz | σ, $sec^{-1}$ | ω, Hz | σ, $sec^{-1}$ | ω, Hz | σ, $sec^{-1}$ |
| 1 | 4.84 | -- | 10.97 | 0.71 | 39.69 | -- |
| 2 | 4.88 | -- | 10.95 | 0.70 | 40.56 | 0.50 |
| 3 | 6.05 | -- | 10.80 | 0.75 | 173.0 | -- |

Table 8 Case 2 Flexbeam/Blade Modal Frequency

| Blade mode | Modal frequency with pitch link installed, Hz | Modal frequency with no pitch link installed, Hz | | |
|---|---|---|---|---|
| | (measured) | (measured) | (calculated) | (error) |
| First flap | 4.88 | 4.69 | 5.21 | +11.1% |
| Second flap | 24.81 | 24.81 | -- | -- |
| First lead-lag | 11.13 | 10.94 | 11.74 | +7.3% |
| First torsion | 38.28 | 19.73 | 18.24 | -7.6% |

Table 9 Pitch Angle and Lead-Lag Damping for Case 1 at 1100 rpm

| θ, deg | $\sigma_\zeta$, $sec^{-1}$ |
|---|---|
| -4.0 | -4.14 |
| -4.0 | -4.08 |
| -4.0 | -3.97 |
| -2.0 | -1.38 |
| -2.0 | -1.62 |
| 0 | -0.864 |
| 0 | -0.756 |
| 2.0 | -0.578 |
| 2.0 | -0.559 |
| 4.0 | -1.19 |
| 4.0 | -1.28 |
| 6.0 | -3.06 |
| 6.0 | -3.17 |
| 6.0 | -3.32 |

Table 10 Pitch Angle and Lead-Lag Damping for Case 2 at 900 rpm[a]

| θ, deg | $\sigma_\zeta$, $sec^{-1}$ |
|---|---|
| -4.0 | -0.646 |
| -4.0 | -0.659 |
| -2.0 | -0.538 |
| -2.0 | -0.559 |
| +4.0 | -0.742 |
| +4.0 | -0.712 |
| +6.0 | -0.781 |
| +6.0 | -0.866 |
| +8.0 | -1.11 |
| +8.0 | -1.008 |

[a]Lead-lag damping was not measured at 0° pitch angle because of a flutter that occurred at the first torsion mode frequency.

Table 11 Pitch Angle and Lead-Lag Damping for Case 3 at 1100 rpm

| $\theta$, deg | $\sigma_\zeta$, $sec^{-1}$ |
|---|---|
| -4.0 | -0.773 |
| -4.0 | -0.732 |
| -2.0 | -0.679 |
| -2.0 | -0.672 |
| 0 | -0.591 |
| 0 | -0.630 |
| +2.0 | -0.713 |
| +2.0 | -0.702 |
| +4.0 | -0.914 |
| +4.0 | -0.893 |
| +6.0 | -1.21 |
| +6.0 | -1.17 |
| +8.0 | -1.47 |
| +8.0 | -1.56 |
| +8.0 | -1.51 |

Table 12 Explanation of Prediction Codes

| ID | Prediction Method | User |
|---|---|---|
| BH | DRAV21 | Bell Helicopter Textron |
| BV | C-90 | Boeing Vertol |
| $HH_1$ | DART | Hughes Helicopters |
| $SA_1$ | G400 | Sikorsky Aircraft |
| $SA_2$ | E927-2 | Sikorsky Aircraft |
| $SA_3$ | E927-3 | Sikorsky Aircraft |
| AL | FLAIR | U.S. Army Aeromechanics Laboratory |

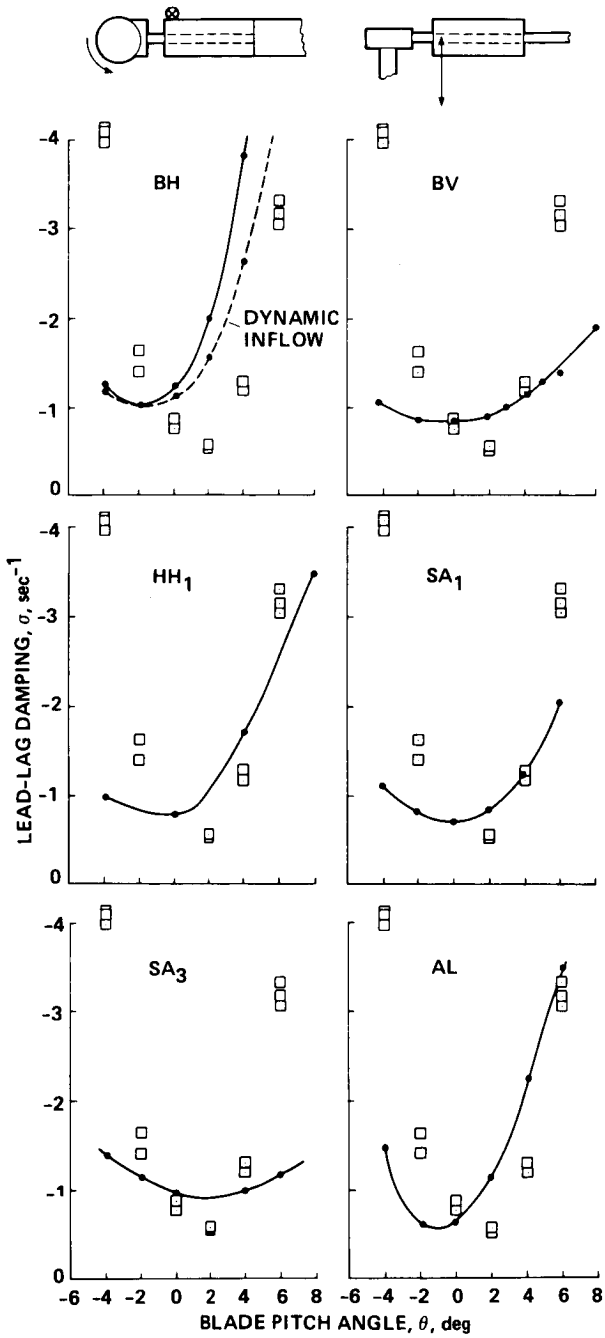


Fig. 7 Individual comparison for Case 1 lead-lag damping.

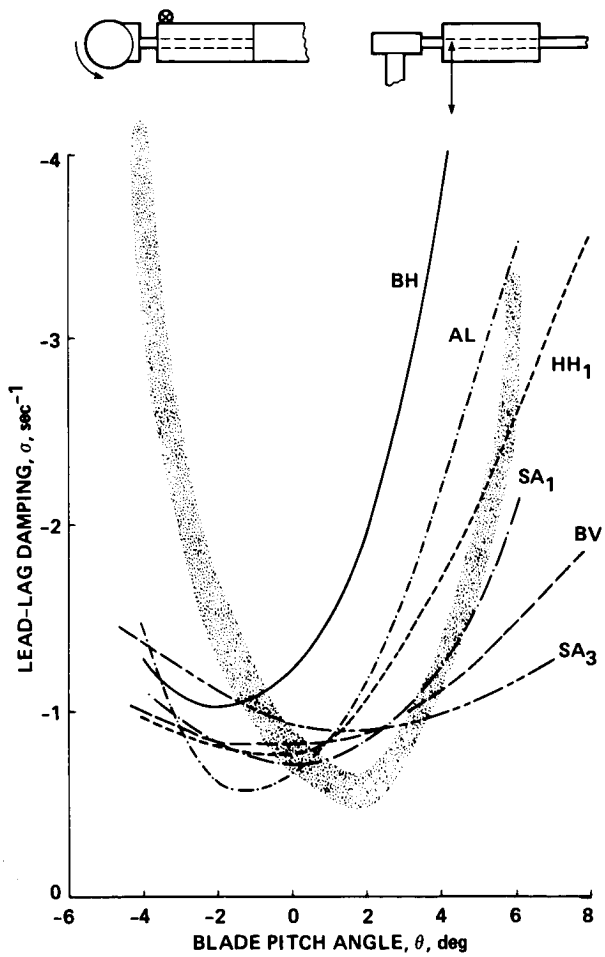


Fig. 8 Composite comparison for Case 1 lead-lag damping.

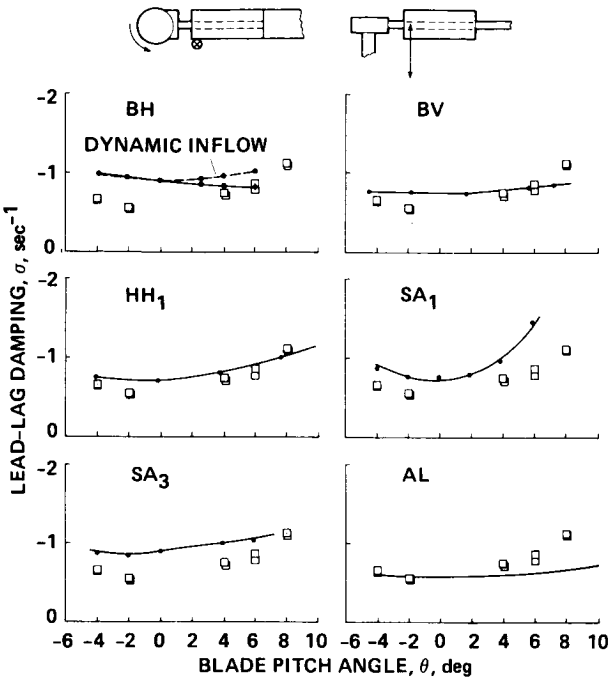


Fig. 9 Individual comparison for Case 2 lead-lag damping.

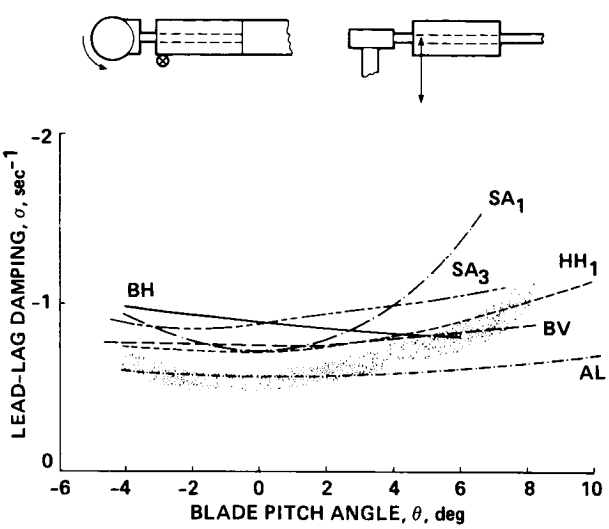


Fig. 10 Composite comparison for Case 2 lead-lag damping.

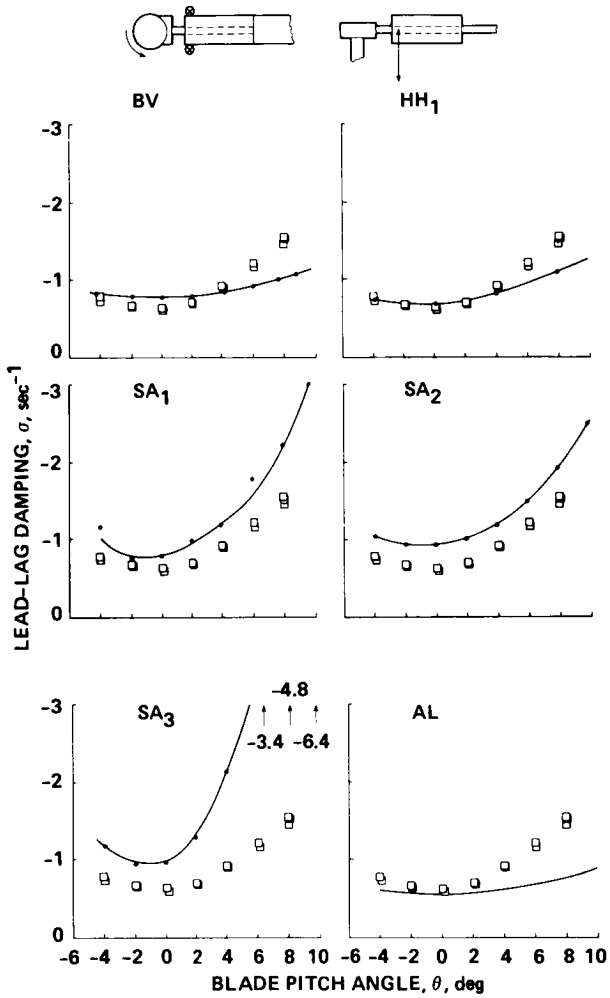


Fig. 11 Individual comparison for Case 3 lead-lag damping.

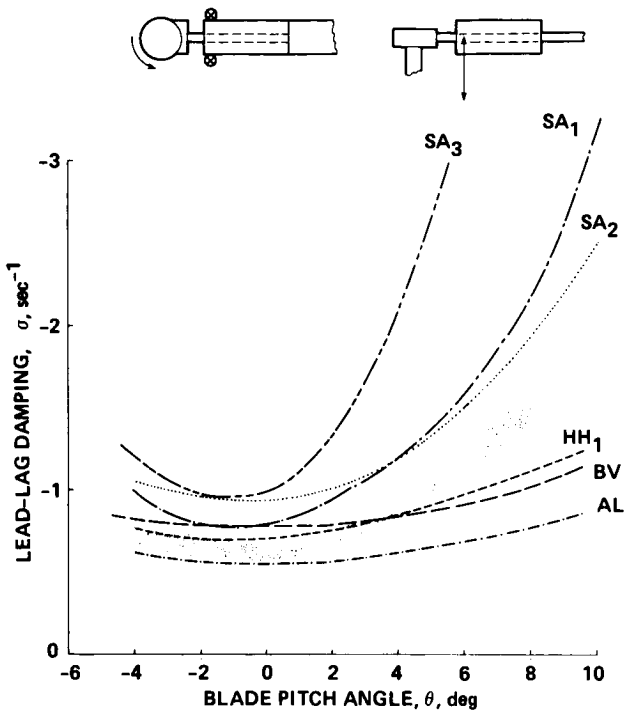


Fig. 12 Composite comparison for Case 3 lead-lag damping.